Received May 18, 2018, accepted June 18, 2018, date of publication June 25, 2018, date of current version July 12, 2018.

*Digital Object Identifier 10.1109/ACCESS.2018.2850146*

# An Uplink Transmission Scheme for Pattern Division Multiple Access Based on DFT Spread Generalized Multi-Carrier Modulation

**XIN BIAN[1,2], JIE TANG[2,3], HONG WANG[1,4], MINGQI LI[2], AND RONGFANG SONG[1,5]**

[1]School of Communications and Information Engineering, Nanjing University of Posts and Telecommunications, Nanjing 210003, China
[2]Shanghai Advanced Research Institute, Chinese Academy of Sciences, Shanghai 201210, China
[3]University of Chinese Academy of Sciences, Beijing 100049, China
[4]National Mobile Communications Research Laboratory, Southeast University, Nanjing 210096, China
[5]Jiangsu Engineering Research Center of Communication and Network Technology, Nanjing University of Posts and Telecommunications, Nanjing 210003, China

Corresponding authors: Mingqi Li (limq@sari.ac.cn) and Rongfang Song (songrf@njupt.edu.cn)

This work was supported in part by the Science and Technology Commission of Shanghai Municipality under Grant 18DZ2203900, in part by the Project of Zhangjiang Hi-Tech District Management Committee under Grant 2016-14, in part by the Open Research Fund of the Jiangsu Engineering Research Center of Communication and Network Technology, NJUPT, in part by the Natural Science Foundation of Jiangsu Province under Grant BK20170910, and in part by the Open Research Foundation of the National Mobile Communications Research Laboratory, Southeast University, under Grant 2018D09.

**ABSTRACT** In order to meet the requirements of high system throughput, massive connectivity, and asynchronous transmission for 5G and beyond, non-orthogonal transmission techniques, including modulation techniques and multiple access techniques, have attracted a great deal of attention in both academia and industry. Traditional non-orthogonal multiple access (NOMA) schemes are investigated mainly based on the orthogonal waveform, i.e., orthogonal frequency-division multiplexing (OFDM). However, OFDM is not the most suitable waveform for the foreseeable mMTC scenarios because it is vulnerable to carrier frequency offset (CFO). To employ the advantages of both NOMA and non-orthogonal waveforms, in this paper, we focus on NOMA transmissions with the non-orthogonal waveform modulation. Specifically, an uplink transmission scheme for pattern-division multiple access (PDMA) based on discrete Fourier transform spread generalized multi-carrier (DFT-S-GMC) modulation, DFT-S-GMC-PDMA for short, is studied. First, implementation schemes of the proposed DFT-S-GMC-PDMA in the time domain and frequency domain are presented, respectively. Second, the equivalent channel response matrix and noise formulas of both implementation schemes are derived. Furthermore, simulation results are given to show that the DFT-S-GMC-PDMA can achieve a comparable performance to PDMA based on discrete Fourier transform spread OFDM (DFT-S-OFDM-PDMA), while the improvement of complexity is less than 3%. system performance under different equalizers and different PDMA patterns are also evaluated where neglectable performance loss is observed. Thanks to the robustness against CFO, the multiple-access interference performance of the DFT-S-GMC-PDMA scheme is about 0.5 dB superior to that of the corresponding the DFT-S-OFDM-PDMA scheme. It indicates by simulation that the proposed DFT-S-GMC-PDMA is robust to CFO at the cost of neglectable performance loss, and thus it is a more attractive candidate for the uplink transmission of mMTC.

**INDEX TERMS** CFO, DFT-S-GMC, 5G, non-orthogonal multiple access, PDMA, waveform modulation.

## I. INTRODUCTION

Enhanced mobile broadband (eMBB), massive machine-type communications (mMTC), and ultra-reliable low-latency communications (URLLC) are three major families of scenarios for the fifth generation (5G) systems [1]–[4]. It is difficult to satisfy the high system throughput with improved spectral efficiency (SE) and massive connectivity in the current communication system. In order to meet these challenging requirements, new multiple access and modulation schemes are explored [5]–[9].

Multiple access techniques have been viewed as the defining feature for each generation of mobile communications. Frequency division multiple access (FDMA), time division multiple access (TDMA), code division multiple

access (CDMA), and orthogonal frequency division multiple access (OFDMA) are used in 1G, 2G, 3G, and 4G, respectively. The philosophy of the access techniques mentioned above is that resource blocks are orthogonally divided in time, frequency, or code domains. Thus, it is easy to implement multi-user detection with minimal interference among adjacent blocks. From the perspective of multi-user information theory, however, orthogonal multiple access (OMA) cannot achieve the optimal system capacity [10] and SE because the orthogonal resource blocks are not fully used. To support enhanced capacity and a large number of concurrent connections in the foreseeable applications, various non-orthogonal multiple access (NOMA) schemes have been proposed [11], [12].

The newly proposed NOMA techniques can be primarily classified into two categories: power-domain NOMA (i.e., PD-NOMA [13]–[15]) and code-domain NOMA, e.g., sparse code multiple access (SCMA) [16], multi-user shared access (MUSA) [17], PDMA [18], etc. The basic idea of NOMA is to schedule multiple users on the same resource block by exploiting the power and/or code domain. By using NOMA, the number of concurrent users is not limited by the number of orthogonal resource blocks, and thus the capacity is significantly improved at the cost of the increase of computational complexity at the receiver.

Besides, as an elegant waveform modulation technique, OFDM, which inherits the advantage of robustness against multipath effects, an easy implementation through fast Fourier transform (FFT) algorithms, and natural combination with multiple-input-multiple-output (MIMO) technique, is exploited in the long-term evolution (LTE) and LTE-Advanced systems [19]. However, traditional OFDM may not be the most suitable waveform for some application scenarios of 5G. In the mMTC scenario, for example, multiple users usually send different types of signals asynchronously over a very narrow bandwidth, while OFDM requires different users be strict-synchronized, otherwise large interference among adjacent subbands will emerge. To cope with the new challenges, various non-orthogonal modulation schemes have been proposed [6], which include filter-bank multi-carrier (FBMC) modulation [20], generalized frequency division multiplexing (GFDM) [21], universal filtered multi-carrier (UFMC) [22], filtered-OFDM (F-OFDM) [23], generalized multicarrier (GMC) [24], DFT-S-GMC [25], etc. Broadly speaking, all the above non-orthogonal modulation schemes belong to filter-bank modulation techniques. The principle of the above modulation schemes is to utilize filtering, pulse shaping, and precoding to reduce the out-of-band (OOB) leakage of OFDM signals, and thus they are robust to time-frequency offset.

There are several surveys studying both the non-orthogonal waveform modulation and non-orthogonal multiple access techniques [26], [27]. In most of the existing works on non-orthogonal transmission techniques, NOMA and non-orthogonal waveform modulation techniques are discussed separately [8], [28]. To exploit the advantages of both NOMA and non-orthogonal waveforms, the combination of NOMA and non-orthogonal waveforms is investigated, on which the relevant references include FBMC-NOMA [29], GFDM-NOMA [30], LDS-FBMC [31], etc. However, they are based on critically sampled filter-bank modulation techniques with inevitable intrinsic interference. To the best of our knowledge, the combination of NOMA and oversampled filter-bank modulation techniques has not been investigated.

DFT-S-GMC is an oversampled filter-bank modulation technique, where neglectable inter-carrier-interference (ICI) is achieved by adding frequency domain guard intervals between subbands [32]. With the flexibility in block-wise data transmission, DFT-S-GMC is also capable of adapting to different lengths of data packets; therefore, system performance, e.g., data processing delay, is improved, especially in the Machine-Type Communication (MTC) class of infrequent and small data packet communication transmission scenario. Additionally, with a DFT precoding operation before the filter-bank transformation, the transmitted signal of DFT-S-GMC has the low peak-to-average ratio (PAPR) characteristic of the single carrier system, which is favorable for improving the power amplifier efficiency of the transmitted signal in the uplink. Meanwhile, different from other NOMA schemes, PDMA designs the transceiver jointly with unequal diversity at the transmitter and equal post-detection diversity at the receiver, which can reap the benefit of the joint design of transmitter and receiver [33]. Motivated by this, we research the combination of PDMA and DFT-S-GMC techniques.

The main contributions of this paper are summarized as follows:

1) This article focuses on the system design of non-orthogonal multiple access based on non-orthogonal waveform modulation schemes. Specifically, a PDMA uplink transmission scheme based on DFT-S-GMC modulation is studied. It is worth mentioning that the performance of DFT-S-GMC in the PDMA scheme is unknown in the existing literature.
2) The time domain and frequency domain realizations of DFT-S-GMC-PDMA are developed, respectively. Accordingly, theoretical expressions of the equivalent channel response matrix and equivalent noise variance of DFT-S-GMC-PDMA are derived, respectively. These derivations facilitate the design of multi-user detection algorithm.
3) A comprehensive performance evaluation is conducted, which includes the overall block error rate (BLER) and spectral efficiency, comparison of different receivers and different PDMA pattern matrices, MAI with CFO, complexity analysis, and PAPR performance. Simulation results show that the proposed DFT-S-GMC-PDMA scheme can achieve a comparable performance to DFT-S-OFDM-PDMA with an acceptable computational complexity. Specifically, with 4 subbands, the improvement of complexity is about 3%. The robustness to CFO of the proposed DFT-S-GMC-PDMA scheme is

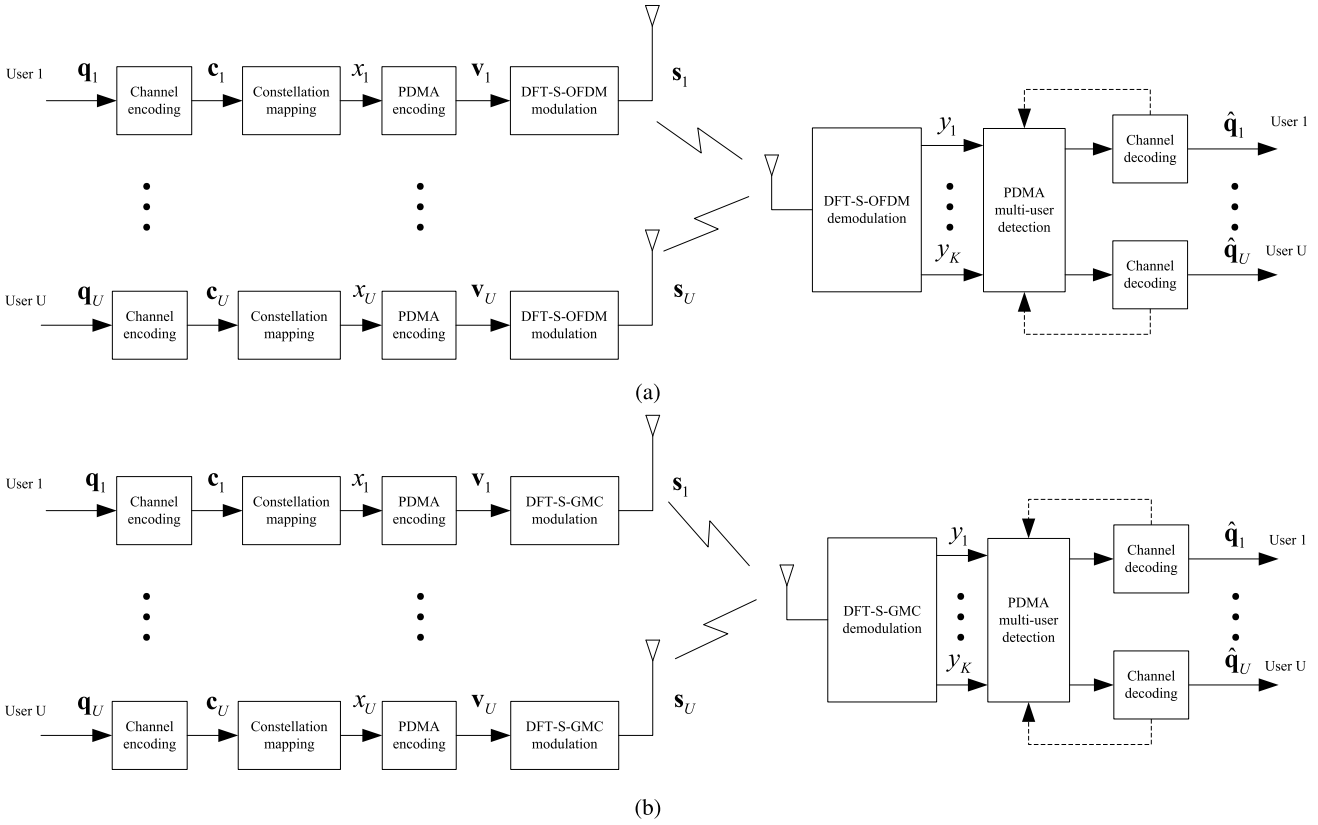


**FIGURE 1.** PDMA uplink system model based on distinguished modulation schemes. (a) DFT-S-OFDM-PDMA; (b) DFT-S-GMC-PDMA.

superior to that of the corresponding DFT-S-OFDM-PDMA scheme. It can be inferred from the performance evaluations that the proposed DFT-S-GMC-PDMA scheme can make a compromise between system performance and computational complexity, and is able to serve as a suitable candidate uplink transmission scheme for mMTC.

The rest of this paper is organized as follows. We first present the traditional PDMA uplink model in Section II, and then the time domain and frequency domain implementations of DFT-S-GMC-PDMA are given in Section III and Section IV, respectively. Performance is evaluated in Section V. Section VI concludes this paper.

*Notations:* Throughout this paper, uppercase and lowercase boldface letters denote matrices and vectors, respectively. $\mathbf{X}^T$ and $\mathbf{X}^H$ denote the transpose and Hermitian transpose of matrix $\mathbf{X}$, respectively. $\mathbf{x}(m)$, $\mathbf{X}_m$, and $\mathbf{X}_{m,n}$ denote the $m^{th}$ element of vector $\mathbf{x}$, $m^{th}$ column of matrix $\mathbf{X}$, and $(m, n)^{th}$ entry of matrix $\mathbf{X}$, respectively. $((\cdot))_Q$ denotes modulo $Q$ operation, round$(\cdot)$ denotes the round operation, and $\mathbb{E}\{\cdot\}$ stands for the expectation operator. $\mathbf{I}_N$ denotes the $N \times N$ identity matrix. $\mathbf{F}_N$ is the $N$-point DFT matrix, i.e., $\mathbf{F}_{n,k} = \frac{1}{\sqrt{K}} e^{-j\frac{2\pi nk}{K}}$ with $\mathbf{F}_N^H \mathbf{F}_N = \mathbf{I}_N$. $diag\{\cdot\}$ denotes a diagonal matrix. $\mathcal{CN}(\mu, \sigma^2)$ denotes a circularly symmetric complex normal distribution with mean $\mu$ and variance $\sigma^2$.

## II. PDMA UPLINK MODEL BASED ON DFT-S-OFDM MODULATION

In this paper, we assume that both transmitter and receiver are equipped with one antenna and are ideally synchronized. An uplink PDMA system based on DFT-S-OFDM modulation, namely DFT-S-OFDM-PDMA, is illustrated on Fig. 1(a). The basic idea of PDMA can be depicted as follows. At the transmitter, the modulated quadratic amplitude modulation (QAM) symbols $x_u$ are mapped onto certain resource blocks through a PDMA encoder and generates the PDMA modulation vector $\mathbf{v}_u$. At the receiver, data of multiplexed users is detected through a multi-user PDMA detector. The detection algorithm is based on message passing algorithm (MPA) or successive interference cancellation (SIC) algorithm [12].

There are $U$ users in the uplink DFT-S-OFDM-PDMA system. For the $u^{th}$ user, the original information bits $\mathbf{q}_u$ are first input to the channel coding module, and then the coded bits $\mathbf{c}_u$ are modulated into the QAM symbols $x_u$. By spreading the user's modulated QAM symbol $x_u$ according to the PDMA pattern $\mathbf{b}_u$, the PDMA modulation vector $\mathbf{v}_u$ of the $u^{th}$ user is expressed as

$$\mathbf{v}_u = \mathbf{b}_u x_u, \quad 1 \le u \le U, \tag{1}$$

where $\mathbf{b}_u = [\mathbf{b}_u(0), \ldots, \mathbf{b}_u(K-1)]^T$ is the $K \times 1$ binary vector with its elements taking values from "0" or "1". "1"

indicates that the users' data is mapped onto the corresponding resource element (RE), and "0" otherwise. The $U$ users' PDMA patterns on $K$ REs constitute a $K \times U$ PDMA pattern matrix $\mathbf{B}_{K,U}$, denoted as [18]

$$\mathbf{B}_{K,U} = [\mathbf{b}_1, \mathbf{b}_2, \ldots, \mathbf{b}_U]. \tag{2}$$

After the DFT-S-OFDM demodulation processing, the signal $\mathbf{y}$ at the base station (BS) side can be depicted as

$$\mathbf{y} = \sum_{u=1}^{U} diag\left(\mathbf{h}_u\right) \mathbf{v}_u + \mathbf{n}, \tag{3}$$

where $\mathbf{n}$ denotes a $K \times 1$ noise plus interference vector at the receiver side, $\mathbf{h}_u = [\mathbf{h}_u(0), \ldots, \mathbf{h}_u(K-1)]^T$ is an uplink channel response with the order $K-1$ for the corresponding REs of the $u^{th}$ user, and $diag(\mathbf{h}_u)$ represents a diagonal matrix with its elements being the vector $\mathbf{h}_u$.

Substituting (1) and (2) into (3), (3) can be rewritten as

$$\mathbf{y} = \mathbf{H}\mathbf{x} + \mathbf{n}, \tag{4}$$

where $\mathbf{x} = [x_1, x_2, \ldots, x_U]^T$, and $\mathbf{H}$ indicates the PDMA equivalent channel response matrix of $U$ users multiplexed on $K$ REs and is denoted by $\mathbf{H} = \mathbf{H}_{ch} \otimes \mathbf{B}_{K,U}$. $\mathbf{H}_{ch} = [\mathbf{h}_1, \mathbf{h}_2, \ldots, \mathbf{h}_U]$, the $(k,u)^{th}$ element of $\mathbf{H}_{ch}$ is the channel response from the $u^{th}$ user to the BS on the $k^{th}$ RE, and $\otimes$ is the Kronecker operator, indicating the element-wise product of two matrices.

Overloading factor is adopted to assess the capability of multiplexing of PDMA in comparison to the corresponding OMA, which is defined as the ratio of the number of multiplexed users to the number of REs for a PDMA pattern. For example, when $K = 2$ and $U = 3$, the overloading factor is $\beta = U/K = 150\%$, which represents that the number of users supported by PDMA is one and a half times that of OMA. The PDMA pattern matrix can be illustrated by

$$\mathbf{B}_{2,3} = \begin{bmatrix} 1 & 1 & 0 \\ 1 & 0 & 1 \end{bmatrix}, \tag{5}$$

and therefore, the corresponding received signal is denoted as

$$\begin{bmatrix} y_1 \\ y_2 \end{bmatrix} = \begin{bmatrix} h_{1,1} & h_{1,2} & 0 \\ h_{2,1} & 0 & h_{2,3} \end{bmatrix} \begin{bmatrix} x_1 \\ x_2 \\ x_3 \end{bmatrix} + \begin{bmatrix} n_1 \\ n_2 \end{bmatrix}. \tag{6}$$

At the receiver, MPA is performed to separate different users' signals. Given the received signal vector $\mathbf{y}$ as the observation and the assumption that the PDMA equivalent channel response matrix $\mathbf{H}$ is available, the optimal detection of $\mathbf{x}$ can be derived by a joint optimal maximum a posteriori (MAP) detection given as

$$\hat{\mathbf{x}} = \arg\max_{\mathbf{x} \in \aleph^U} p\left(\mathbf{x}|\mathbf{y}, \mathbf{H}\right), \tag{7}$$

where $\aleph^U$ represents the constellation alphabet of $U$ users, and $p(\cdot)$ denotes the posterior probability function.

By using the Bayes' rule, (7) can be approximately translated into a simper solution

$$\hat{x}_u = \arg\max_{\alpha \in \aleph} \sum_{\mathbf{x} \in \aleph^U, x_k = \alpha} P(\mathbf{x}) \prod_{k \in \lambda_v(u)} p\left(y_k|\mathbf{x}\right), \tag{8}$$

where $\aleph$ and $\lambda_v(u)$ represent constellation alphabet and the index set corresponding to the PDMA pattern of the $u^{th}$ user, respectively. The problem can be solved by applying the MPA algorithm onto the underlying factor-graph [34].

## III. PDMA UPLINK MODEL BASED ON DFT-S-GMC TIME DOMAIN IMPLEMENTATION

### A. TRANSMITTER

In this section, we focus on the transceiver design of PDMA uplink system based on DFT-S-GMC modulation. As is shown in Fig. 1(b), the modulation module of DFT-S-OFDM is replaced by DFT-S-GMC. We attempt to derive the equivalent channel response matrix and the equivalent noise vector for the PDMA uplink transmission based on the time-domain DFT-S-GMC (i.e., TD-DFT-S-GMC) modulation and demodulation shown in Fig. 2(a) and Fig. 2(b), respectively.

For simplicity of analysis, it is assumed that the uplink time synchronization is achieved. It can be implemented by random access channel (RACH) procedure initialized from the user side and signalling procedure at the BS side. Under such circumstances, the transmit time intervals of multiple users are no more than one symbol length. It is also assumed that the channel impulse response of each user is approximately the same, which is feasible when a plurality of users with similar geographic locations intend to access the network. Based on the above assumptions, the independent PDMA patterns of $U$ users on $K$ REs superposed at the DFT-S-GMC modulation side can be viewed as the PDMA pattern matrix $\mathbf{B}_{K,U}$. In the following, we will omit the subscript of $\mathbf{B}_{K,U}$ for concision, and therefore, the input signal of DFT-S-GMC can be denoted as

$$\mathbf{a}_d = \mathbf{B}\mathbf{x}_d, \tag{9}$$

where $\mathbf{a}_d = [\mathbf{a}_d(0), \mathbf{a}_d(1), \ldots, \mathbf{a}_d(K-1)]^T$ with $d \in \{0, \ldots, D-1\}$ denotes the $d^{th}$ superposed sub-vector with size $K \times 1$, and $\mathbf{x}_d = \left[x_{d,1}, x_{d,2}, \ldots, x_{d,U}\right]^T$ is the $d^{th}$ original data sub-vector of the $U$ users.

After $K$-point DFT spreading, $\mathbf{a}_d$ becomes

$$\mathbf{e}_d = \mathbf{F}_K \mathbf{a}_d. \tag{10}$$

Then the $K \times 1$ vector $\mathbf{e}_d$ is mapped to $M$ subbands signal vector $\mathbf{e}'_d = \left[\mathbf{e}'_d(0), \mathbf{e}'_d(1), \ldots, \mathbf{e}'_d(M-1)\right]^T$ according to the mapping rule

$$\mathbf{e}'_d(m) = \begin{cases} \mathbf{e}_d\left(k'\right), & m = k_0 + k'R, \\ 0, & m \neq k_0 + k'R. \end{cases} \tag{11}$$

Note that $M$ is the total number of subbands of DFT-S-GMC, $k_0$ is the initial subband offset, and $R$ is the repetition factor. For DFT-S-GMC systems, both distributed and centralized

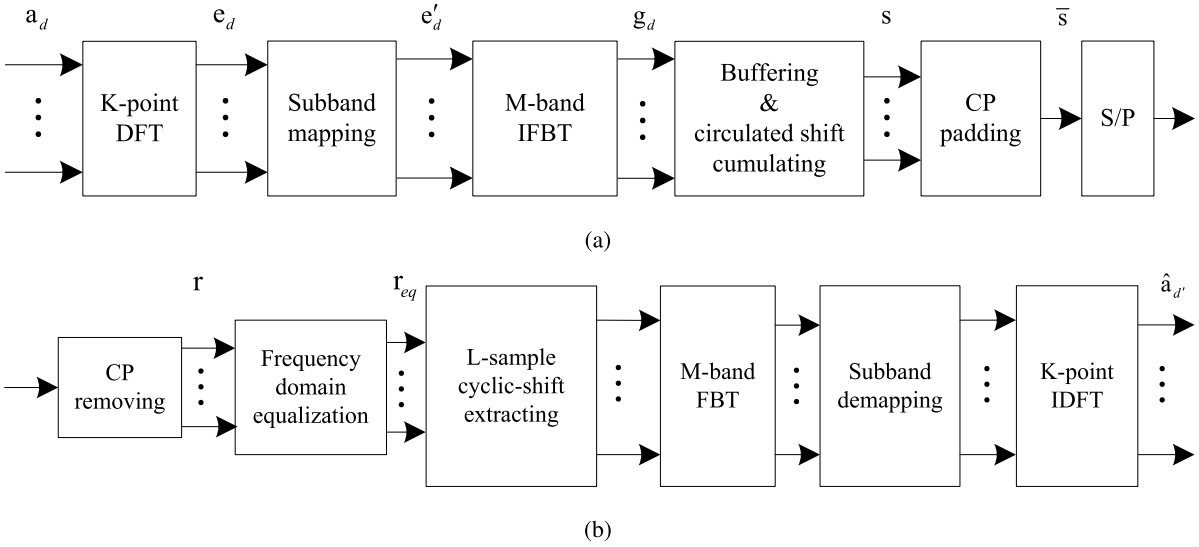


**FIGURE 2.** DFT-S-GMC time domain implementation. (a) transmitter; (b) receiver.

mapping rules are supported, representing $R$ greater than 1 and equal to 1, respectively.

Equation (11) can be compactly rewritten as

$$\mathbf{e}'_d = \mathbf{T}_{M,K}\mathbf{e}_d, \tag{12}$$

where $\mathbf{T}_{M,K}$ is the $M \times K$ subbband mapping matrix with its element being "0" or "1", and $\mathbf{T}^T_{M,K}\mathbf{T}_{M,K} = \mathbf{I}_K$.

Conducting an inverse filter-bank transform (IFBT) operation on the sub-band mapped signal $\mathbf{e}'_d$ yields

$$\mathbf{g}_d = \Upsilon_L \Gamma_{L,M} \mathbf{F}^H_M \mathbf{e}'_d, \tag{13}$$

where $\Upsilon_L = diag\{f(0), f(1), \ldots, f(L-1)\}$ is the $L \times L$ time domain filtering matrix with $f(n)$ serving as its diagonal elements, and the $N_1$-repetition matrix is given by $\Gamma_{L,M} = [\underbrace{\mathbf{I}_M, \mathbf{I}_M, \ldots, \mathbf{I}_M}_{N_1}]^T$. $f(n)$ is the prototype filter with length $L_0$ and can be extended to $L$ point with $L = N_1 M$ by zero padding operation. The prototype filter is normalized in energy, i.e., $\sum_{l=0}^{L-1} |f(l)|^2 = 1$.

Then, a zero padding is performed on each IFBT symbol to form a $Q$-sample data block, i.e.,

$$\tilde{\mathbf{g}}_d(n) = \begin{cases} \mathbf{g}_d(n), & 0 \leqslant n \leqslant L-1, \\ 0, & L \leqslant n \leqslant Q-1, \end{cases} \tag{14}$$

where $Q = D \times N$, $D$ denotes the data block length transmitted on each subband, and $N$ represents the cyclic shift interval.

Next, $D$ successive $Q$-sample data blocks are buffered, cyclically shifted, and accumulated. Then, the output signal is given by

$$\mathbf{s}(n) = \sum_{d=0}^{D-1} \tilde{\mathbf{g}}_d((n-dN))_Q, \quad 0 \leqslant n \leqslant Q-1. \tag{15}$$

Equation (15) can be written in a matrix form given as

$$\mathbf{s} = \sum_{d=0}^{D-1} \Omega_{d;Q,L}\mathbf{g}_d, \tag{16}$$

where $\Omega_{Q,L} = \left[\mathbf{I}_L \ \mathbf{0}_{L\times(Q-L)}\right]^T$ denotes the buffering matrix, and $\Omega_{d;Q,L}$ is the circularly shifted version of $\Omega_{Q,L}$ with $dL$ elements downwards.

Substituting (9), (10), (11), (13) into (16) yields the transmitted signal vector

$$\mathbf{s} = \sum_{d=0}^{D-1} \Omega_{d;Q,L}\Upsilon_L\Gamma_{L,M}\mathbf{F}^H_M\mathbf{T}_{M,K}\mathbf{F}_K\mathbf{B}\mathbf{x}_d. \tag{17}$$

A CP of size $L_{CP}$ is added to the transmitted signal vector $\mathbf{s}$ in (17), thus generating the CP-added transmitted signal $\mathbf{N} = [\mathbf{s}(Q-L_{CP}), \ldots, \mathbf{s}(Q-1), \mathbf{s}(0), \ldots, \mathbf{s}(Q-1)]^T$, which is then launched into the wireless channel.

*Remark 1:* Note from (17) that when $L = M = N$, $D = 1$, and $f(n) = 1$, we obtain $\mathbf{s} = \mathbf{F}^H_M\mathbf{T}_{M,K}\mathbf{F}_K\mathbf{B}\mathbf{x}_d$, which is the transmitter signal vector of DFT-S-OFDM-PDMA illustrated in Fig. 1(a). When the DFT spread module is omitted, we derive the original PDMA signal vector based on OFDM modulation, i.e., $\mathbf{s} = \mathbf{F}^H_M\mathbf{T}_{M,K}\mathbf{B}\mathbf{x}_d$. In other words, DFT-S-OFDM-PDMA can be viewed as a special case of DFT-S-GMC-PDMA.

### B. RECEIVER

Assume $\mathbf{N}$ is transmitted through the multipath fading channel with an $L_{CP}$-tap finite impulse response (FIR) $\xi = [\xi(0), \ldots, \xi(L_{CP}-1)]^T$. After the cyclic prefix is removed, the received signal vector at the receiver, $\mathbf{r} = [\mathbf{r}(0), \ldots, \mathbf{r}(Q-1)]^T$, can be expressed as

$$\mathbf{r} = \Xi\mathbf{s} + \mathbf{z}, \tag{18}$$

where $\Xi$ denotes the $Q \times Q$ circular channel matrix with the first column given by $\left[\xi^T \ \mathbf{0}^T\right]^T$, and the noise vector satisfies $\mathbf{z} \sim \mathcal{CN}\left(\mathbf{0}, \sigma_z^2\mathbf{I}\right)$.

We adopt the frequency-domain equalization approach at the receiver end. Applying Fourier transform to both sides of (18) yields

$$\tilde{\mathbf{r}} = \Psi\tilde{\mathbf{s}} + \tilde{\mathbf{z}}, \tag{19}$$

where $\tilde{\mathbf{r}} = \mathbf{F}_Q\mathbf{r}$, $\tilde{\mathbf{s}} = \mathbf{F}_Q\mathbf{s}$, $\tilde{\mathbf{z}} = \mathbf{F}_Q\mathbf{z}$ are $Q \times 1$ vectors, $\Psi = diag\left\{\Psi\left(0\right), \Psi\left(1\right), \ldots, \Psi\left(Q-1\right)\right\}$ is the $Q \times Q$ matrix with its diagonal elements being the $Q$-point frequency channel responses, and the $q^{th}$ diagonal element is given by $\Psi\left(q\right) = \sum_{n=0}^{L_{CP}-1} \xi\left(n\right) \exp\left(-j2\pi qn/Q\right)$.

After $Q$-point one-tap equalization in the frequency domain, we obtain

$$\tilde{\mathbf{r}}_{eq} = \mathbf{W}\Psi\mathbf{F}_Q\mathbf{s} + \mathbf{W}\mathbf{F}_Q\mathbf{z}, \tag{20}$$

where the equalization coefficient matrix $\mathbf{W}$ is expressed as $\mathbf{W} = diag\left\{w_0, w_1, \ldots . w_q, \ldots, w_{Q-1}\right\}$. The elements in $\mathbf{W}$ depend on the type of equalizer. For minimum mean squared error (MMSE) equalization, $w_q = \frac{\Psi(q)}{|\Psi(q)|^2+\sigma_z^2}$; For zero-forced (ZF) equalization, $w_q = 1/|\Psi\left(q\right)|$.

The equalized frequency domain signal is then transformed back to the time domain, and thus we obtain $\mathbf{r}_{eq} = \mathbf{F}_Q^H\tilde{\mathbf{r}}_{eq}$, which can be presented by

$$\mathbf{r}_{eq} = \mathbf{F}_Q^H\mathbf{W}\Psi\mathbf{F}_Q\mathbf{s} + \mathbf{F}_Q^H\mathbf{W}\mathbf{F}_Q\mathbf{z}, \tag{21}$$

where $\mathbf{r}_{eq}$ is then demodulated by $L$-sample cyclic-shifted data extraction, $M$-band filter-bank transform (FBT), sub-band demapping, and $K$-point DFT operations. Now the $d'^{th}$ symbol detection vector $\hat{\mathbf{a}}_{d'}$ after demodulation can be derived as

$$\hat{\mathbf{a}}_{d'} = \mathbf{F}_K^H\mathbf{T}_{M,K}^T\mathbf{F}_M\Gamma_{L,M}^T\Upsilon_L^H\Omega_{d';Q,L}^H\mathbf{r}_{eq}. \tag{22}$$

Substituting (21) into (22) yields

$$\hat{\mathbf{a}}_{d'} = \tilde{\mathbf{a}}_{d'} + \bar{\mathbf{a}}_{d'} + \tilde{\mathbf{z}}_{d'}, \tag{23}$$

where $\tilde{\mathbf{a}}_{d'}$, $\bar{\mathbf{a}}_{d'}$, and $\tilde{\mathbf{z}}_{d'}$ are the desired detection vector, the interference vector between different IFBT symbols, and the equivalent channel noise vector, respectively. The expressions of $\tilde{\mathbf{a}}_{d'}$, $\bar{\mathbf{a}}_{d'}$, and $\tilde{\mathbf{z}}_{d'}$ are given as

$$\begin{aligned}\tilde{\mathbf{a}}_{d'} &= \mathbf{F}_K^H\mathbf{T}_{M,K}^T\mathbf{F}_M\Gamma_{L,M}^T\Upsilon_L^H\Omega_{d';Q,L}^H\mathbf{F}_Q^H \\ &\quad\cdot\mathbf{W}\Psi\mathbf{F}_Q\Omega_{d';Q,L}\Upsilon_L\Gamma_{L,M}\mathbf{F}_M^H\mathbf{T}_{M,K}\mathbf{F}_K\mathbf{B}\mathbf{x}_{d'}, \quad (24)\\ \bar{\mathbf{a}}_{d'} &= \mathbf{F}_K^H\mathbf{T}_{M,K}^T\mathbf{F}_M\Gamma_{L,M}^T\Upsilon_L^H\Omega_{d';Q,L}^H\mathbf{F}_Q^H\mathbf{W}\Psi\mathbf{F}_Q \\ &\quad\cdot\sum_{d=0,d\neq d'}^{D-1}\Omega_{d;Q,L}\Upsilon_L\Gamma_{L,M}\mathbf{F}_M^H\mathbf{T}_{M,K}\mathbf{F}_K\mathbf{B}\mathbf{x}_d, \quad (25)\\ \tilde{\mathbf{z}}_{d'} &= \mathbf{F}_K^H\mathbf{T}_{M,K}^T\mathbf{F}_M\Gamma_{L,M}^T\Upsilon_L^H\Omega_{d';Q,L}^H\mathbf{F}_Q^H\mathbf{W}\mathbf{F}_Q\mathbf{z}. \quad (26)\end{aligned}$$

### C. EQUIVALENT CHANNEL RESPONSE MATRIX AND NOISE ANALYSIS

As seen in Appendix A, we can rewrite the $d'^{th}$ symbol detection vector $\hat{\mathbf{a}}_{d'}$ after demodulation as

$$\hat{\mathbf{a}}_{d'} = \mathbf{H}_{eq1}\mathbf{x}_{d'} + \mathbf{z}_{eq1}, \tag{27}$$

where the equivalent channel response matrix and the equivalent noise vector are

$$\mathbf{H}_{eq1} = \mathbf{F}_K^H\Lambda_{sig}\mathbf{F}_K\mathbf{B}, \tag{28}$$

and

$$\mathbf{z}_{eq1} = \left[\mathbf{z}_{eq1}\left(0\right), \ldots, \mathbf{z}_{eq1}\left(K-1\right)\right]^T, \tag{29}$$

respectively. The $k^{th}$ element of $\mathbf{z}_{eq1}$ is denoted as $\mathbf{z}_{eq1}\left(k\right) = \sigma_{int1}^2 + \sigma_z^2\zeta_1\left(k\right)$. Now we can detect the superposed signal vector $\mathbf{x}$ by the multi-user detection algorithm, i.e.,

$$\hat{\mathbf{x}}_{d'} = \arg\max_{\mathbf{x}_{d'}\in\mathfrak{A}^U} p\left(\mathbf{x}_{d'}|\hat{\mathbf{a}}, \mathbf{H}_{eq1}\right). \tag{30}$$

## IV. PDMA UPLINK MODEL BASED ON DFT-S-GMC FREQUENCY DOMAIN IMPLEMENTATION

### A. TRANSMITTER

It can be observed from (13) and (15) that the transmitted symbols are multiplexed within each DFT-S-GMC symbol over both time and frequency domains. Performing $Q$-point DFT on the DFT-S-GMC modulation signal yields [35]

$$\mathbf{s}\left(n\right) = \sum_{q=0}^{Q-1}\sum_{m=0}^{M-1}\mathbf{P}_{m,q}\sum_{d=0}^{D-1}\mathbf{e}_d'\left(m\right)\exp\left(\frac{-j2\pi qd}{D}\right)\exp\left(\frac{j2\pi qn}{Q}\right), \tag{31}$$

where $\mathbf{P}_{m,q}$ is the $q^{th}$ element of the $m^{th}$ subband filter frequency response $\mathbf{P}_m$, denoted by

$$\mathbf{P}_{m,q} = \sum_{n=0}^{Q-1} f\left(n\right)\exp\left(j2\pi mn/M\right)\exp\left(-j2\pi qn/Q\right). \tag{32}$$

The transmitted signal (31) can be written in the matrix form given as

$$\mathbf{s} = \mathbf{F}_Q^H\sum_{d=0}^{D-1}\Phi_{Q,d}\mathbf{P}_{Q,M}\mathbf{T}_{M,K}\mathbf{F}_K\mathbf{B}\mathbf{x}_d, \tag{33}$$

where $\mathbf{P}_{Q,M} = [\mathbf{P}_0, \mathbf{P}_1, \ldots, \mathbf{P}_{M-1}]$ is the $Q \times M$ sub-band filter matrix with the subband filter frequency response vector given by $\mathbf{P}_m = [\mathbf{P}_m\left(0\right), \ldots, \mathbf{P}_m\left(Q-1\right)]^T$, the element of $\mathbf{P}_m$ is shown in (32), and $\Phi_{Q,d}$ is a diagonal matrix, i.e., $\Phi_{Q,d} = diag\left\{1, e^{-j2\pi d/D}, \ldots, e^{-j2\pi d(Q-1)/D}\right\}$. Detailed frequency domain implementation of DFT-S-GMC (i.e., FD-DFT-S-GMC) transmitter can be found in [35].

*Remark 2:* It is observed from (31) that the energy of the subband filter frequency response $\mathbf{P}_m$ spreads over the whole band or all the frequency domain equalization (FDE) subcarriers, and therefore the multi-subband summation operation

will result in a high degree of complexity. Note that the frequency response of the prototype filter $f(n)$ has a steep spectrum skirt, and thus we can infer that the energy of each subband filter frequency response is mainly distributed in the minority frequency components. If the frequency components with the small amount of energy are ignored, the complexities of the multi-subband summation and the frequency domain windowing operation will be dramatically reduced, and thus the multi-subband summation calculation can be simplified to the subcarrier-mapping operation. In this case, the effective length of the $m^{th}$ subband filter frequency response $\mathbf{P}_m$ is reduced from $Q$-point to $G_m$-point, where $G_m$ is the number of frequency components that the $m^{th}$ subband occupies. A detailed design method of $G_m$ can be found in [36]. In addition, detailed analysis of complexity will be given in Section V.

### B. RECEIVER

At the receiver, after the removal of CP and FDE operations, the output signal vector can be expressed as

$$\mathbf{r} = \mathbf{W}\Psi\mathbf{F}_Q\mathbf{F}_Q^H \sum_{d=0}^{D-1} \Phi_{Q,d}\mathbf{P}_{Q,M}\mathbf{T}_{M,K}\mathbf{F}_K\mathbf{B}\mathbf{x}_d + \mathbf{W}\mathbf{F}_Q\mathbf{z}, \tag{34}$$

where $\Psi = diag\left\{\Psi_0, \ldots, \Psi_q, \ldots, \Psi_{Q-1}\right\}$, $\Psi_q$ is the frequency response of the $q^{th}$ subcarrier for FDE, and $\mathbf{W}$ is the equalization coefficient matrix.

Without loss of generality, herein we just analyze the first IFBT symbol. Actually, the signal-to-interference-plus-noise ratio (SINR) for any IFBT symbol is the same [37], and therefore the detected signal vector can be denoted as

$$\begin{aligned}\hat{\mathbf{a}}_0 &= \mathbf{F}_K^H\mathbf{T}_{M,K}^T\mathbf{P}_{Q,M}^H\Phi_{Q,0}^H\mathbf{r} \\ &= \mathbf{F}_K^H\mathbf{T}_{M,K}^T\mathbf{P}_{Q,M}^H\Phi_{Q,0}^H\mathbf{W}\Psi\mathbf{F}_Q\mathbf{F}_Q^H\sum_{d=0}^{D-1}\Phi_{Q,d}\mathbf{P}_{Q,M} \\ &\quad \cdot\mathbf{T}_{M,K}\mathbf{F}_K\mathbf{B}\mathbf{x}_d \\ &\quad + \mathbf{F}_K^H\mathbf{T}_{M,K}^T\mathbf{P}_{Q,M}^H\Phi_{Q,0}^H\mathbf{W}\mathbf{F}_Q\mathbf{z}. \end{aligned} \tag{35}$$

Equation (35) can also be depicted as

$$\hat{\mathbf{a}}_0 = \tilde{\mathbf{a}}_0 + \bar{\mathbf{a}}_0 + \tilde{\mathbf{z}}_0, \tag{36}$$

where $\tilde{\mathbf{a}}_0$ is the desired detect vector, $\bar{\mathbf{a}}_0$ and $\tilde{\mathbf{z}}_0$ are respectively the interference vector of different QAM symbols and the equivalent noise vector in the $0^{th}$ IFBT symbol, and they are given by

$$\begin{aligned}\tilde{\mathbf{a}}_0 &= \mathbf{F}_K^H\mathbf{T}_{M,K}^T\mathbf{P}_{Q,M}^H\Phi_{Q,0}^H\mathbf{W}\Psi\mathbf{F}_Q\mathbf{F}_Q^H\Phi_{Q,0}\mathbf{P}_{Q,M} \\ &\quad \cdot\mathbf{T}_{M,K}\mathbf{F}_K\mathbf{B}\mathbf{x}_0, \end{aligned} \tag{37}$$

$$\begin{aligned}\bar{\mathbf{a}}_0 &= \mathbf{F}_K^H\mathbf{T}_{M,K}^T\mathbf{P}_{Q,M}^H\Phi_{Q,0}^H\mathbf{W}\Psi\sum_{d'=1}^{D-1}\Phi_{Q,d'}\mathbf{P}_{Q,M} \\ &\quad \cdot\mathbf{T}_{M,K}\mathbf{F}_K\mathbf{B}\mathbf{x}_{d'}, \end{aligned} \tag{38}$$

and

$$\tilde{\mathbf{z}}_0 = \mathbf{F}_K^H\mathbf{T}_{M,K}\mathbf{P}_{Q,M}^H\Phi_{Q,0}^H\mathbf{W}\mathbf{F}_Q\mathbf{z}. \tag{39}$$

respectively.

**TABLE 1. Simulation assumptions.**

| Parameter | Value |
|---|---|
| Carrier | 2 GHz |
| Sampling frequency | 7.68 MHz |
| Occupied bandwidth | 56 subcarriers/4 subbands |
| Resource mapping | Localized/Distributed |
| Modulation coding rate | QPSK 1/2; LTE Turbo |
| Data block length | 14 |
| Prototype filter | SRRC |
| Filter length | 448 |
| Mobile speed | 3 km/h |
| Antenna configuration | 1Tx 2Rx |
| Channel model | AWGN/Rayleigh |
| Channel estimation | Ideal |
| Uplink overload factor | 150%/200% |
| PDMA pattern type | According to [33] |
| Uplink average SNR | The same for all users |
| Detection algorithm | MPA/SIC |

### C. EQUIVALENT CHANNEL RESPONSE MATRIX AND NOISE ANALYSIS

Equation (36) can be rewritten as

$$\hat{\mathbf{a}}_0 = \mathbf{H}_{eq2}\mathbf{x}_0 + \mathbf{z}_{eq2}, \tag{40}$$

where the equivalent channel matrix and equivalent noise vector for FD-DFT-S-GMC-PDMA can be derived from the Appendix B, i.e.,

$$\mathbf{H}_{eq2} = \mathbf{F}_K^H\Delta_{sig}\mathbf{F}_K\mathbf{B}, \tag{41}$$

and

$$\mathbf{z}_{eq2} = \left[\mathbf{z}_{eq2}(0), \ldots, \mathbf{z}_{eq2}(K-1)\right]^T, \tag{42}$$

respectively. The $k^{th}$ element of $\mathbf{z}_{eq2}$ is denoted as $\mathbf{z}_{eq2}(k) = \sigma_{int2}^2 + \sigma_z^2\zeta_2(k)$. The multi-user detection algorithm based on BP can be utilized to detect the desired vector $\hat{\mathbf{x}}_0$ given by

$$\hat{\mathbf{x}}_0 = \arg\max_{\mathbf{x}_0 \in \aleph^U} p\left(\mathbf{x}_0 | \hat{\mathbf{a}}_0, \mathbf{H}_{eq2}\right). \tag{43}$$

## V. SIMULATION RESULTS AND PERFORMANCE EVALUATION

### A. SIMULATION PARAMETERS

In this section, we provide some numerical results to evaluate the link-level performance of the proposed DFT-S-GMC-PDMA scheme; PDMA uplink scheme based on DFT-S-OFDM modulation is considered as a benchmark. Simulation parameters are summarized in Table 1, which is compliant with the new radio (NR) specifications [38].

For the parameter selections in PDMA, the pattern matrix is of size $4 \times 6$ or $4 \times 8$, which represents that there are 6 or 8 users superposed onto 4 REs and the overloading factor $\beta = 150\%$ and $\beta = 200\%$, respectively. The design criteria of the PDMA pattern matrix follow the principle

**TABLE 2.** PDMA pattern matrix.

| Type | PDMA pattern matrix with $\beta = 150\%$ |
|---|---|
| Pattern1 | $\begin{bmatrix} 1 & 0 & -0.250+0.433i & -0.433-0.250i & -0.354+0.354i & -0.433+0.250i \\ 0 & 1 & -0.250-0.433i & 0.250+0.433i & -0.500i & 0.250-0.433i \\ 0 & 0 & 0.500 & -0.500i & 0.354+0.354i & 0.500i \\ 0 & 0 & -0.250+0.433i & -0.250+0.433i & -0.500 & -0.250-0.433i \end{bmatrix}$ |
| Pattern2 | $\begin{bmatrix} 1 & 0 & 0 & 0.577 & -0.577 & 0 \\ 0 & 1 & 0 & 0.577 & 0.577 & 0 \\ 0 & 0 & 1 & 0.577 & 0.577 & 0 \\ 0 & 0 & 0 & 0 & 0 & 1 \end{bmatrix}$ |
| Pattern3 | $\begin{bmatrix} 0 & 0.707 & 0.707 & 0 & 0.707 & 0 \\ 0.707 & 0 & 0.707 & 0 & 0 & 0.707 \\ 0 & 0.707 & 0 & 0.707 & 0 & 0.707 \\ 0.707 & 0 & 0 & 0.707 & 0.707 & 0 \end{bmatrix}$ |

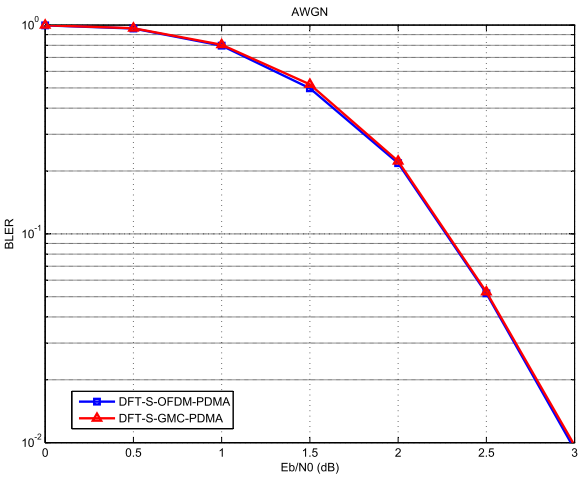


**FIGURE 3.** AWGN performance comparison.

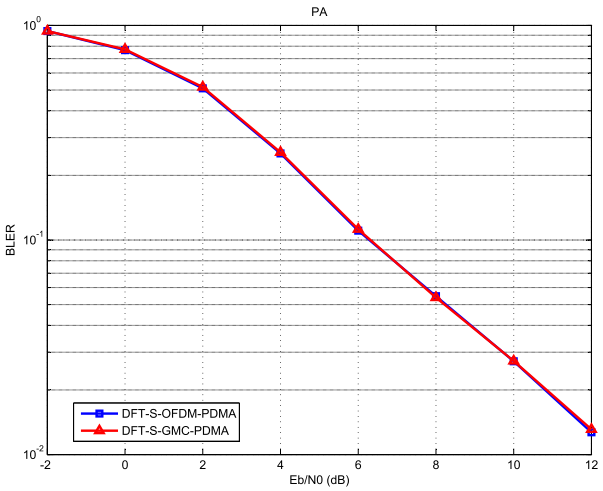


**FIGURE 4.** Rayleigh-fading channel performance comparison.

in [33]. Three PDMA patterns, denoted as Pattern1, Pattern2, Pattern3 are chosen for mMTC (i.e. Type1-3 in [33]) with $\beta = 150\%$ and $\beta = 200\%$, respectively. A specific example of PDMA pattern matrix is illustrated in Table 2. To evaluate the performance of different receiver algorithms, MPA, symbol-level SIC (SL-SIC), codeword-level SIC (CW-SIC), and Turbo-SIC are taken into consideration. For the parameters of DFT-S-GMC, the number of subbands $M$ is 20, the data block length $D$ on each subband is 14. Square-root raised cosine (SRRC) filter is used as the prototype filter $f(n)$ with roll-off factor 0.2 and filter length 448. To ensure the same amount of transmitted data of both systems, 56 subcarriers and 4 subbands are set for DFT-S-OFDM-PDMA and DFT-S-GMC-PDMA, respectively. Both localized and distributed resource mapping rules are utilized. Perfect channel estimation is also assumed. 10000 frames are conducted in the simulation.

### B. OVERALL BLER AND SPECTRAL EFFICIENCY PERFORMANCE

Fig. 3 shows the BLER performance of the DFT-S-GMC-PDMA under AWGN channel, where Pattern3 and MPA detection algorithm are employed. The overall BLER performance comparison between DFT-S-OFDM-PDMA and DFT-S-GMC-PDMA in a four-path Rayleigh-fading channel [39] by Monte Carlo method [40] is illustrated in Fig. 4. It can be seen from Fig. 3 and Fig. 4 that when the localized resource mapping is adopted, the proposed DFT-S-GMC-PDMA is capable of achieving the BLER performance very close to that of DFT-S-OFDM-PDMA due to the negligible ICI.

Fig. 5 provides the SE performance of DFT-S-GMC-PDMA in a six-path Rayleigh-fading channel [39] with $\beta = 150\%$. It can be seen from Fig. 5 that a 50% SE gain can be obtained when the signal-to-noise ratio (SNR) is high.

### C. COMPARISON OF DIFFERENT RECEIVERS AND DIFFERENT PDMA PATTERN MATRICES

Performance of different PDMA receivers of DFT-S-OFDM-PDMA and DFT-S-GMC-PDMA is illustrated in Fig. 6, where Pattern3 is adopted under 150% overloaded scenario. We can observe from Fig. 6 that the system performance with MPA detection algorithm is about 1 dB better than those of all

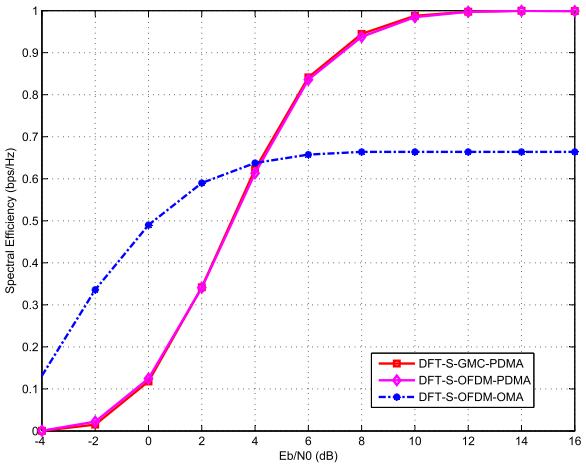


**FIGURE 5.** Spectral efficiency performance comparison.

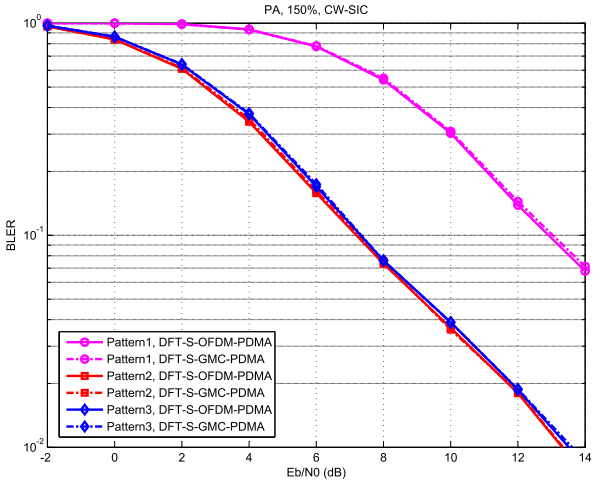


**FIGURE 7.** Performance comparison of different PDMA pattern matrices.

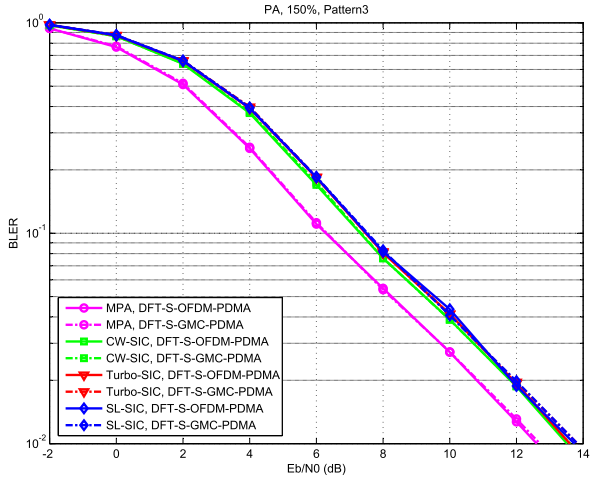


**FIGURE 6.** Performance comparison of different PDMA receivers.

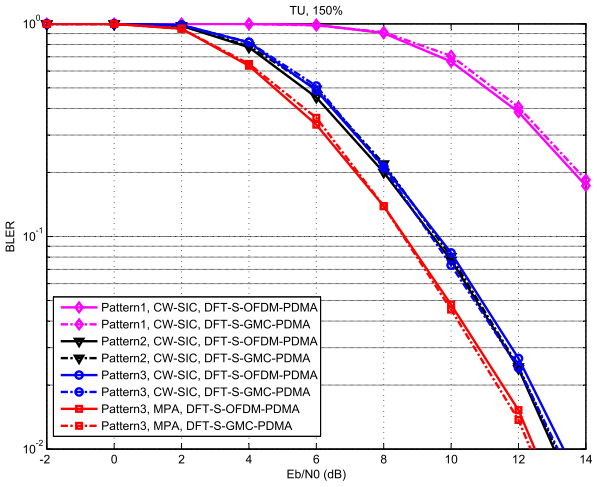


**FIGURE 8.** Performance comparison of different PDMA pattern matrices.

the other SIC receivers. It is because error propagation of SIC receivers has a negative effect on the system performance. On the other hand, we can also observe that the system performance with CW-SIC is slightly better than that with Turbo-SIC or SL-SIC. The reason is that channel coding is able to correct most errors in CW-SIC.

Performance of different PDMA pattern matrices of both DFT-S-OFDM-PDMA and DFT-S-GMC-PDMA in PA and TU channels with 150% overloaded are shown in Fig. 7 and Fig. 8, respectively. It can be seen that, when CW-SIC is adopted, the order of the performance from the highest to lowest is Pattern2, Pattern3, Pattern1, respectively. The reason behind this can be owing to the differences in correlation metric of PDMA patterns in different PDMA matrices [33].

Performance of different PDMA pattern matrices of both DFT-S-OFDM-PDMA and DFT-S-GMC-PDMA in PA and TU channels with 200% overloaded under CW-SIC receiver are shown in Fig. 9 and Fig. 10, respectively. We can observe the similar relationship in terms of performance of all the PDMA patterns. Additionally, the gap between performance of Pattern2 (Pattern3) in Fig. 9 and Fig. 10 is larger than that in Fig. 7 and Fig. 8, respectively. This is due to the fact that as the number of superposed users increases, the error propagation effect becomes severe.

In summary, we can also observe from Fig. 6 to Fig. 10 that DFT-S-OFDM-PDMA and DFT-S-GMC-PDMA can achieve almost the same BLER performance for different receivers, different PDMA patterns, and different overloading factors.

### D. MAI PERFORMANCE WITH CFO

In an asynchronous multi-user transmission scenario, MAI occurs and causes system performance loss when there is a time-frequency synchronization error. We evaluate the MAI performance caused by CFO in this subsection.

Considering an uplink PDMA network of $K' = 18$ users, decomposed into 3 groups with 6 users per group, labeled by $G0$, $G1$, and $G2$, respectively. Each group occupies 4 subbands for DFT-S-GMC-PDMA or 56 subcarriers for DFT-S-OFDM-PDMA. Note that the resources that different groups occupy are contiguously distributed, i.e., the resource mapping method for each group of users are either

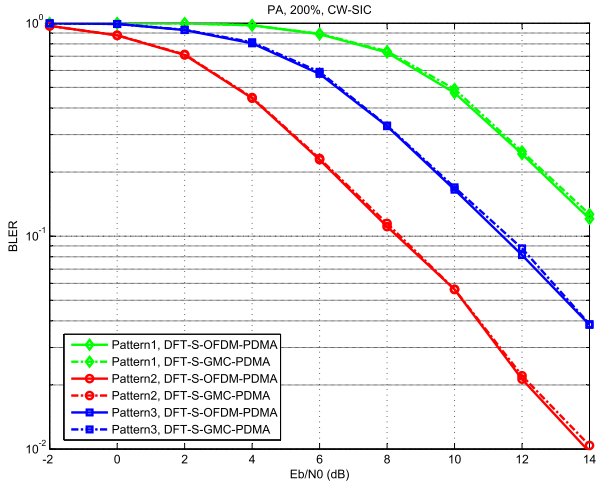


**FIGURE 9.** Performance comparison of different PDMA pattern matrices.

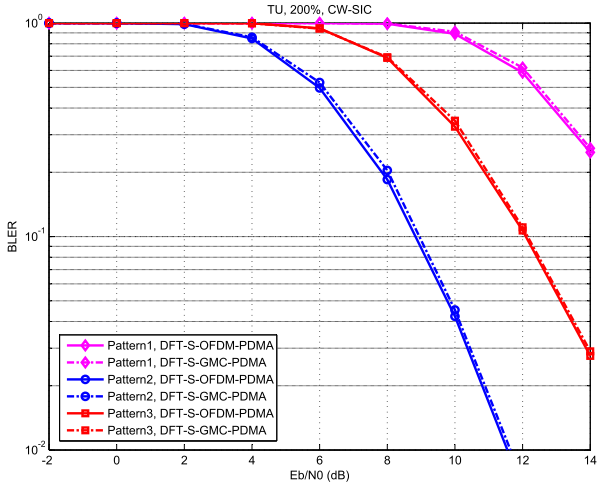


**FIGURE 10.** Performance comparison of different PDMA pattern matrices.

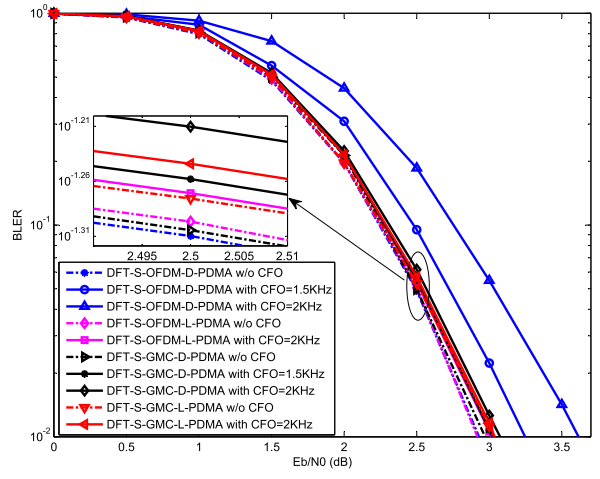


**FIGURE 11.** MAI performance comparison with CFO.

localized (denoted by DFT-S-OFDM-L-PDMA) or distributed (denoted by DFT-S-OFDM-D-PDMA and DFT-S-GMC-D-PDMA, respectively). Without loss of generality,

**TABLE 3.** Modulation complexity comparison.

| | DFT-S-OFDM | TD-DFT-S-GMC | FD-DFT-S-GMC |
|---|---|---|---|
| DFT spreading | 2DKlogK+4K$I$ | 2DKlogK | 2DKlogK |
| data modulation | 2QlogQ | D(2L+2MlogM) | 4K*round(Q/M)+ 4K$I$+2QlogQ |
| K = 1 | 9316 | 17024 | 9380 |
| K = 4 | 9840 | 17248 | 10096 |
| K = 32 | 16896 | 21504 | 18944 |

**TABLE 4.** Demodulation complexity comparison.

| | DFT-S-OFDM | TD-DFT-S-GMC | FD-DFT-S-GMC |
|---|---|---|---|
| DFT despreading | 2DKlogK+4K$I$ | 2DKlogK | 2DKlogK |
| FDE | 2QlogQ | 4QlogQ | 2QlogQ |
| data demodulation | 2QlogQ | D(2L+2MlogM) | 4K*round(Q/M) + 4K$I$ |
| K = 1 | 9316 | 35456 | 9380 |
| K = 4 | 9840 | 35680 | 10096 |
| K = 32 | 16896 | 39936 | 18944 |

**TABLE 5.** Total transceiver complexity comparison.

| | DFT-S-OFDM | TD | Increment | FD | Increment |
|---|---|---|---|---|---|
| K = 1 | 18632 | 52480 | 181.7% | 18760 | 0.7% |
| K = 4 | 19680 | 52928 | 168.9% | 20192 | 2.6% |
| K = 32 | 33792 | 61440 | 81.8% | 37888 | 12.1% |

assume group $G1$ experiences CFO with 1.5KHz or 2KHz, while the other two groups do not. Fig. 11 shows the overall MAI performance with CFO for users in group $G0$ over AWGN channel. It is seen from Fig. 11 that in the case of no CFO for group $G1$, the BLER curves of the three schemes is almost the same. The system performance degrades in the case of CFO = 1.5KHz (2KHz) for DFT-S-OFDM-D-PDMA with the SNR loss up to 0.7dB at BLER=0.01. Moreover, for DFT-S-OFDM-D-PDMA and DFT-S-GMC-PDMA, the SNR loss is no more than 0.2dB. Hence, the performance of DFT-S-OFDM-L-PDMA is the best under CFO, followed by DFT-S-GMC-D-PDMA, DFT-S-GMC-L-PDMA, and DFT-S-OFDM-D-PDMA in sequence. This is because only the subcarriers at the edge of the continuous spectrum that group $G0$ users occupy suffer from CFO introduced by the group $G1$ for DFT-S-OFDM-L-PDMA, while most of the occupied subcarriers can demodulate the symbols ideally. For DFT-S-OFDM-D-PDMA, each distributed subcarrier over the occupied spectrum suffers from CFO. Thanks to the subband mapping, for DFT-S-GMC-D-PDMA, only the edge of occupied subband subjects to CFO introduced by group $G1$ users, and symbols inside the subbands can be demodulated correctly.

### E. COMPLEXITY ANALYSIS

In this subsection, we analyze the complexity for DFT-S-OFDM-PDMA, TD-DFT-S-GMC-PDMA, and FD-DFT-S-GMC-PDMA. The complexity needed, calculated by

**TABLE 6.** CM performance comparison between DFT-S-OFDM-PDMA and DFT-S-GMC-PDMA.

| | DFT-S-OFDM-OMA | DFT-S-GMC-OMA | DFT-S-OFDM-PDMA | DFT-S-GMC-PDMA |
|---|---|---|---|---|
| occupied subcarriers/subbands | QPSK | QPSK | QPSK | QPSK |
| K = 56/4 | 1.07 | 1.63 | 2.32 | 2.46 |

real multiplication numbers, for modulation at the transmitter side, demodulation at the receiver side, and the whole link are listed in Table 3, Table 4, and Table 5, respectively. Notice that, in Table 5, TD and FD are short for TD-DFT-S-GMC-PDMA and FD-DFT-S-GMC-PDMA, respectively.

As to $D = 14$, the 14-point DFT can be implemented by seven 2-point DFTs and two 7-point DFTs. The 512-point and 4-point DFT use the base 2-FFT algorithm, while the 7-point DFT employs the Winograd Fourier transform algorithm (requires 9 complex multiplications) [41]. $I$ in Table 3 and Table 4 denotes the number of complex multiplications required for 14-point DFT, i.e., the number of complex multiplications is 25. In general, one complex multiplication requires 4 real multiplications and 2 real additions. Since the computational complexity of addition is one order of magnitude lower than multiplication, the comparison of complexity here does not include the calculation of addition. In addition, the division by the frequency-domain equalization is not taken into account. Note that the only difference between two proposed schemes is in the realization methods of the underlying waveform modulation, while the PDMA signal transmission is the same. Therefore, the complexity of belief propagation (BP) multi-user detection algorithm is also not included, about which interested readers can find details in [18] and [33].

As can be seen from Table 5, the total real multiplication required by TD-DFT-S-GMC is very large, increased by 181.7%, 168.9%, and 81.8%, respectively. However, FD-DFT-S-GMC requires 18760, 20192, and 37888 real multiplications for the occupied subband(s) of 1, 4, and 32, respectively, and the complexity is respectively increased by only 0.7%, 2.6%, and 12.1% compared to DFT-S-OFDM. The computational complexity required for FD-DFT-S-GMC is significantly reduced.

Fig. 12 shows the performance comparison between time domain and frequency domain transceivers in Rayleigh-fading channel with QPSK modulation. We can observe from Fig. 12 that the reduced-complexity FD-DFT-S-GMC scheme can achieve almost the same BLER performance as that of TD-DFT-S-GMC. Therefore, we can infer that the SNR loss caused by the simplified reconstruction in the frequency domain, within the system's practical working SNR range, has a negligible effect on the system performance.

### F. PAPR AND CM PERFORMANCE

Fig. 13 shows the complementary cumulative distribution function (CCDF) of PAPR for OMA and PDMA based on DFT-S-OFDM and DFT-S-GMC, respectively. It can be observed from Fig. 13 that the DFT-S-GMC modulation

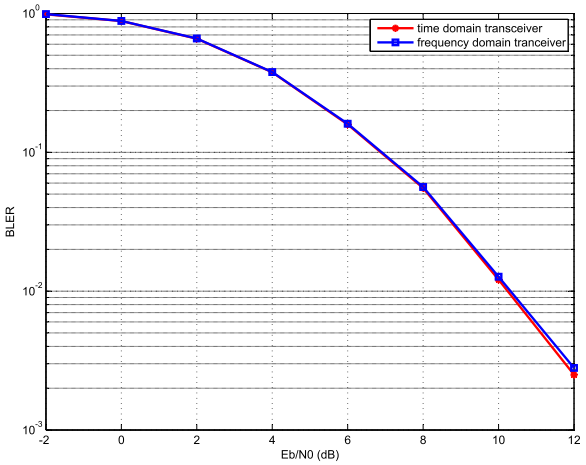


**FIGURE 12.** Performance comparison between time domain and frequency domain transceivers.

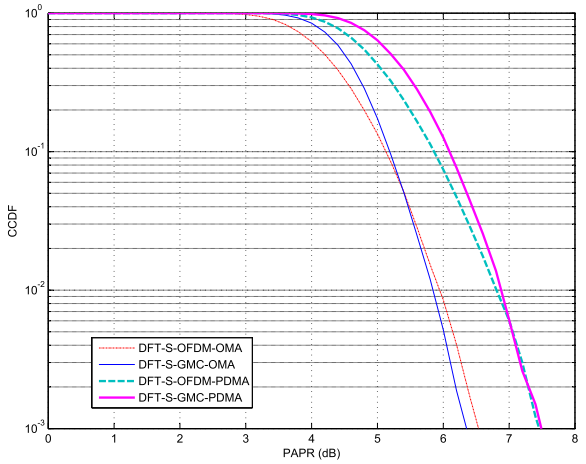


**FIGURE 13.** PAPR performance comparison.

will suffer from PAPR enhancement compared with DFT-S-OFDM modulation. Furthermore, the gap between two above modulation schemes becomes smaller in the case of PDMA transmission, which is a similar case for cubic measurement (CM) performance illustrated in Table 6, although the PAPR of PDMA is 1 dB higher than OMA.

## VI. CONCLUSION

The design of uplink transmission scheme for PDMA based on DFT-S-GMC modulation was developed. We first introduced the time domain and frequency domain transceiver structures of DFT-S-GMC-PDMA, and then gave the equivalent channel response matrix and noise formulas, respec-

tively. After that, we provided extensive numerical results to evaluate the performance of the proposed DFT-S-GMC-PDMA schemes. Simulation results showed that the proposed DFT-S-GMC-PDMA could achieve almost the same BLER and SE performance as that of DFT-S-OFDM-PDMA with 4 subbands; system performance under different receivers and different PDMA patterns showed neglectable performance loss; in terms of MAI performance with CFO, the DFT-S-GMC-D-PDMA behaved better than the corresponding DFT-S-OFDM-D-PDMA; complexity analysis showed that the computational complexity required for FD-DFT-S-GMC-PDMA was at an acceptable level when the occupied bandwidth was relatively narrow; for PAPR performance, both DFT-S-OFDM-PDMA and DFT-S-GMC-PDMA suffered from PAPR enhancement compared to that of OMA. In summary, the proposed DFT-S-GMC-PDMA can make a balance between the system performance and computational complexity, thus it is suitable for the uplink transmission for mMTC.

## APPENDIX A
## DERIVATION OF TIME DOMAIN EQUIVALENT CHANNEL AND NOISE COVARIANCE

We will simplify (24). Denote the product of the matrices between $\mathbf{F}_K^H$ and $\mathbf{F}_K$ on the right side of (24) as

$$\Lambda_{sig} = \mathbf{T}_{M,K}^T \mathbf{F}_M \Gamma_{L,M}^T \Upsilon_L^H \Omega_{d';Q,L}^H \mathbf{F}_Q^H \cdot \mathbf{W} \Psi \mathbf{F}_Q \Omega_{d';Q,L} \Upsilon_L \Gamma_{L,M} \mathbf{F}_M^H \mathbf{T}_{M,K}. \quad (44)$$

Note that the non-diagonal elements of $\Lambda_{sig}$ are very small, and their impacts on system performance can be neglected; therefore, $\Lambda_{sig}$ can be approximated as a diagonal matrix, i.e., $\Lambda_{sig} \approx diag\{\lambda_1(0), \lambda_1(1), \ldots, \lambda_1(K-1)\}$, where $\lambda_1(k) = \sum_{\beta=0}^{N_1-1} |f(k+\beta M)|^2 w_{k+\beta M} \Psi(k+\beta M)$. It can be seen that the matrix $\Lambda_{sig}$ is related to the prototype filter, the practical channel frequency response, and the equalization method. In this case, (24) can be rewritten as

$$\tilde{\mathbf{a}}_{d'} = \mathbf{F}_K^H \Lambda_{sig} \mathbf{F}_K \mathbf{B} \mathbf{x}_{d'}. \quad (45)$$

Similarly, denote the product of the matrices between $\mathbf{F}_K^H$ and $\mathbf{F}_K$ on the right side of (25) as

$$\Lambda_{int} = \mathbf{T}_{M,K}^T \mathbf{F}_M \Gamma_{L,M}^T \Upsilon_L^H \Omega_{d';Q,L}^H \mathbf{F}_Q^H \cdot \mathbf{W} \Psi \mathbf{F}_Q \Omega_{d;Q,L} \Upsilon_L \Gamma_{L,M} \mathbf{F}_M^H \mathbf{T}_{M,K}. \quad (46)$$

Since $\Lambda_{int}$ can also be approximated as a diagonal matrix, i.e., $\Lambda_{int} \approx diag\{\mu_1(0), \mu_1(1), \ldots, \mu_1(K-1)\}$, $\mu_1(k)$ is the $k^{th}$ diagonal element of $\Lambda_{int}$, denoted by $\sum_{\beta=0}^{N_1-1} f(k+\beta M) f\left(k+\beta M-d'N\right) w_{k+\beta M} \Psi(k+\beta M)$. It can be observed that $\Lambda_{int}$ is the function of the prototype filter, the actual channel frequency response, and the noise variance. In such case, (25) can be denoted as

$$\bar{\mathbf{a}}_{d'} = \sum_{d=0,d\neq d'}^{D-1} \mathbf{F}_K^H \Lambda_{int} \mathbf{F}_K \mathbf{B} \mathbf{x}_d. \quad (47)$$

We assume that the transmitted signal $\mathbf{x}_d$ is i.i.d. and normalized in power, and then the average interference power can be expressed as [42]

$$\begin{aligned}
&\mathbb{E}\{\mathbf{tr}\left(\tilde{\mathbf{a}}_{d'} \tilde{\mathbf{a}}_{d'}^H\right)\} \\
&= \sum_{d=0,d\neq d'}^{D-1} \mathbb{E}\{\mathbf{tr}\left(\mathbf{F}_K^H \Lambda_{int} \mathbf{F}_K \mathbf{B} \mathbf{x}_d \mathbf{x}_d^H \mathbf{B}^H \mathbf{F}_K^H \Lambda_{int}^H \mathbf{F}_K\right)\} \\
&= \sum_{d=0,d\neq d'}^{D-1} P_x \mathbf{tr}\left(\mathbf{F}_K^H \Lambda_{int} \mathbf{F}_K \mathbf{B} \mathbf{B}^H \mathbf{F}_K^H \Lambda_{int}^H \mathbf{F}_K\right) \\
&= \sigma_{int1}^2. \quad (48)
\end{aligned}$$

To derive the noise covariance matrix, we first compute the expectation of $\tilde{\mathbf{z}}_{d'} \tilde{\mathbf{z}}_{d'}^H$, i.e.,

$$\begin{aligned}
&\mathbb{E}\{\tilde{\mathbf{z}}_{d'} \tilde{\mathbf{z}}_{d'}^H\} \\
&= \mathbb{E}\{\mathbf{F}_K^H \mathbf{T}_{M,K}^T \mathbf{F}_M \Gamma_{L,M}^T \Upsilon_L^H \Omega_{d';Q,L}^H \mathbf{F}_Q^H \mathbf{W} \mathbf{F}_Q \mathbf{z} \\
&\quad \cdot \mathbf{z}^H \mathbf{F}_Q^H \mathbf{W}^H \mathbf{F}_Q \Omega_{d';Q,L} \Upsilon_L \Gamma_{L,M} \mathbf{F}_M^H \mathbf{T}_{M,K} \mathbf{F}_K\} \\
&= \mathbb{E}\{\mathbf{z}\mathbf{z}^H\} \mathbf{F}_K^H \mathbf{T}_{M,K}^T \mathbf{F}_M \Gamma_{L,M}^T \Upsilon_L^H \Omega_{d';Q,L}^H \mathbf{F}_Q^H \mathbf{W} \mathbf{F}_Q \\
&\quad \cdot \mathbf{F}_Q^H \mathbf{W}^H \mathbf{F}_Q \Omega_{d';Q,L} \Upsilon_L \Gamma_{L,M} \mathbf{F}_M^H \mathbf{T}_{M,K} \mathbf{F}_K \\
&= \sigma_z^2 \Lambda_{noise}, \quad (49)
\end{aligned}$$

where $\Lambda_{noise}$ can be also approximated as a diagonal matrix, i.e., $\Lambda_{noise} \approx diag\{\zeta_1(0), \zeta_1(1), \ldots, \zeta_1(K-1)\}$. $\zeta_1(k)$ is the $k^{th}$ diagonal element of $\Lambda_{noise}$, expressed as $\zeta_1(k) = \sum_{\beta=0}^{N_1-1} |f(k+\beta M)|^2 w_{k+\beta M}^2 \Psi(k+\beta M)$.

Eventually, the detection vector in (23) can be rewritten as

$$\hat{\mathbf{a}}_{d'} = \mathbf{H}_{eq1} \mathbf{x}_{d'} + \mathbf{z}_{eq1}, \quad (50)$$

where the equivalent channel matrix and the equivalent noise vector are

$$\mathbf{H}_{eq1} = \mathbf{F}_K^H \Lambda_{sig} \mathbf{F}_K \mathbf{B}, \quad (51)$$

and

$$\mathbf{z}_{eq1} = \left[\mathbf{z}_{eq1}(0), \ldots, \mathbf{z}_{eq1}(K-1)\right]^T, \quad (52)$$

respectively. The $k^{th}$ element of $\mathbf{z}_{eq1}$ is denoted as $\mathbf{z}_{eq1}(k) = \sigma_{int1}^2 + \sigma_z^2 \zeta_1(k)$.

## APPENDIX B
## DERIVATION OF FREQUENCY DOMAIN EQUIVALENT CHANNEL AND NOISE COVARIANCE

Similarly, (37) can be simplified as

$$\tilde{\mathbf{a}}_0 = \mathbf{F}_K^H \Delta_{sig} \mathbf{F}_K \mathbf{B} \mathbf{x}_0, \quad (53)$$

where matrix $\Delta_{sig}$ can be viewed as a diagonal matrix, i.e., $\Delta_{sig} \approx diag\{\lambda_2(0), \lambda_2(1), \ldots, \lambda_2(K-1)\}$, since the value of non-diagonal elements is very small. The $k^{th}$ diagonal element of $\Delta_{sig}$ is expressed as $\lambda_2(k) = \sum_{q=l_k}^{l_k+G_k-1} |\mathbf{P}_{k,q}|^2 w_q \Psi(q)$. Note that herein the lower and upper limits of the summing operation is $l_k$ and $l_k + G_k - 1$, respectively. $l_k$ denotes the FDE subcarrier offset corresponding to the $k^{th}$ subband, while $G_k$ denotes the occupied subcarriers of each subband.

Furthermore, (38) can be depicted as

$$\bar{\mathbf{a}}_0 = \sum_{d'=1}^{D-1} \mathbf{F}_K^H \Delta_{int} \mathbf{F}_K \mathbf{B} \mathbf{x}_{d'}, \tag{54}$$

where interference matrix $\Delta_{int}$ is approximated as a diagonal matrix, $\Delta_{int} \approx diag\{\mu_2(0), \mu_2(1), \ldots, \mu_2(K-1)\}$. The $k^{th}$ diagonal element of $\Delta_{int}$ is given by $\mu_2(k) = \sum_{q=l_k}^{l_k+G_k-1} \left|\mathbf{P}_{k,q}\right|^2 \exp\left(-j2\pi qd'/D\right) w_q \Psi(q)$.

The interference power of $\bar{\mathbf{a}}_0$ can be derived by

$$\begin{aligned}
&\mathbb{E}\{\mathbf{tr}\left(\bar{\mathbf{a}}_0 \bar{\mathbf{a}}_0^H\right)\} \\
&= \mathbb{E}\{\mathbf{x}_{d'} \mathbf{x}_{d'}^H\} \sum_{d'=1}^{D-1} \mathbf{tr}\left(F_K^H \Delta_{int} \mathbf{F}_K \mathbf{B}\mathbf{B}^H \mathbf{F}_K^H \Delta_{int}^H \mathbf{F}_K\right) \\
&= \sum_{d'=1}^{D-1} \mathbf{tr}\left(\mathbf{F}_K^H \Delta_{int} \mathbf{F}_K \mathbf{B}\mathbf{B}^H \mathbf{F}_K^H \Delta_{int}^H \mathbf{F}_K\right) \\
&= \sigma_{int2}^2.
\end{aligned} \tag{55}$$

The covariance matrix of the noise item, $\tilde{\mathbf{z}}_0$, can be figured out by

$$\begin{aligned}
&\mathbb{E}\{\tilde{\mathbf{z}}_0 \tilde{\mathbf{z}}_0^H\} \\
&= \mathbb{E}\{\mathbf{F}_K^H \mathbf{P}_{Q,K}^H \Phi_{Q,0}^H \mathbf{W} \mathbf{F}_Q \mathbf{z}\mathbf{z}^H \mathbf{F}_Q^H \mathbf{W}^H \Phi_{Q,0} \mathbf{P}_{Q,K} \mathbf{F}_K\} \\
&= \mathbb{E}\{\mathbf{z}\mathbf{z}^H\} \mathbf{F}_K^H \mathbf{P}_{Q,K}^H \Phi_{Q,0}^H \mathbf{W} \mathbf{F}_Q \mathbf{F}_Q^H \mathbf{W}^H \Phi_{Q,0} \mathbf{P}_{Q,K} \mathbf{F}_K \\
&= \sigma_z^2 \Delta_{noise},
\end{aligned} \tag{56}$$

where $\Delta_{noise} \approx diag\{\zeta_2(0), \zeta_2(1), \ldots, \zeta_2(K-1)\}$, and the $k^{th}$ element of $\Delta_{noise}$ is denoted by $\zeta_2(k) = \sum_{q=l_k}^{l_k+G_k-1} \left|\mathbf{P}_{k,q}\right|^2 w_q^2 \Psi(q)$.

Now the detected vector $\hat{\mathbf{a}}_0$ can be indicated as

$$\hat{\mathbf{a}}_0 = \mathbf{H}_{eq2} \mathbf{x}_0 + \mathbf{z}_{eq2}. \tag{57}$$

The equivalent channel matrix and equivalent noise vector in (57) is expressed as

$$\mathbf{H}_{eq2} = \mathbf{F}_K^H \Delta_{sig} \mathbf{F}_K \mathbf{B}, \tag{58}$$

and

$$\mathbf{z}_{eq2} = \left[\mathbf{z}_{eq2}(0), \ldots, \mathbf{z}_{eq2}(K-1)\right]^T, \tag{59}$$

respectively. The $k^{th}$ element of $\mathbf{z}_{eq2}$ is denoted as $\mathbf{z}_{eq2}(k) = \sigma_{int2}^2 + \sigma_z^2 \zeta_2(k)$.

## ACKNOWLEDGMENT

The authors would like to thank the anonymous reviewers for reviewing the manuscript and for their constructive remarks.

## REFERENCES


[1] J. G. Andrews *et al.*, "What will 5G be?" *IEEE J. Sel. Areas Commun.*, vol. 32, no. 6, pp. 1065–1082, Jun. 2014.

[2] "IMT vision—Framework and overall objectives of the future development of IMT for 2020 and beyond," ITU-R, Geneva, Switzerland, Tech. Rep. M.2083-0, Sep. 2015.

[3] *Study on Scenarios and Requirements for Next Generation Access Technologies*, document TR 38.913, 3GPP, Mar. 2017.

[4] M. Shafi *et al.*, "5G: A tutorial overview of standards, trials, challenges, deployment, and practice," *IEEE J. Sel. Areas Commun.*, vol. 35, no. 6, pp. 1201–1221, Jun. 2017.

[5] X. Zhang, L. Chen, J. Qiu, and J. Abdoli, "On the waveform for 5G," *IEEE Commun. Mag.*, vol. 54, no. 11, pp. 74–80, Nov. 2016.

[6] Y. Medjahdi *et al.*, "On the road to 5G: Comparative study of physical layer in MTC context," *IEEE Access*, vol. 5, pp. 26556–26581, 2017.

[7] Z. Ding, X. Lei, G. K. Karagiannidis, R. Schober, J. Yuan, and V. K. Bhargava, "A survey on non-orthogonal multiple access for 5G networks: Research challenges and future trends," *IEEE J. Sel. Areas Commun.*, vol. 35, no. 10, pp. 2181–2195, Oct. 2017.

[8] Y. Liu, Z. Qin, M. Elkashlan, Z. Ding, A. Nallanathan, and L. Hanzo, "Nonorthogonal multiple access for 5G and beyond," *Proc. IEEE*, vol. 105, no. 12, pp. 2347–2381, Dec. 2017.

[9] H. Wang and R. Song, "MMSE precoding with configurable sizes for GFDM systems," in *Proc. 9th Int. Conf. Wireless Commun. Signal Process. (WCSP)*, Oct. 2017, pp. 1–6.

[10] D. Tse and P. Viswanath, *Fundamentals of Wireless Communications*, 1st ed. Cambridge, U.K.: Cambridge Univ. Press, 2005.

[11] L. Dai, B. Wang, Y. Yuan, S. Han, C. L. I, and Z. Wang, "Non-orthogonal multiple access for 5G: Solutions, challenges, opportunities, and future research trends," *IEEE Commun. Mag.*, vol. 53, no. 9, pp. 74–81, Sep. 2015.

[12] Y. Wang, B. Ren, S. Sun, S. Kang, and X. Yue, "Analysis of non-orthogonal multiple access for 5G," *China Commun.*, vol. 13, no. 2, pp. 52–66, Dec. 2016.

[13] Y. Saito, Y. Kishiyama, A. Benjebbour, T. Nakamura, A. Li, and K. Higuchi, "Non-orthogonal multiple access (NOMA) for cellular future radio access," in *Proc. 77th IEEE VTC-Spring*, Dresden, Germany, Jun. 2013, pp. 1–5.

[14] S. M. R. Islam, N. Avazov, O. A. Dobre, and K.-S. Kwak, "Power-domain non-orthogonal multiple access (NOMA) in 5G systems: Potentials and challenges," *IEEE Commun. Surveys Tuts.*, vol. 19, no. 2, pp. 721–742, 2nd Quart., 2017.

[15] H. Wang, R. Zhang, R. Song, and S.-H. Leung, "A novel power minimization precoding scheme for MIMO-NOMA uplink systems," *IEEE Commun. Lett.*, vol. 22, no. 5, pp. 1106–1109, May 2018.

[16] L. Lei, C. Yan, G. Wenting, Y. Huilian, W. Yiqun, and X. Shuangshuang, "Prototype for 5G new air interface technology SCMA and performance evaluation," *China commun.*, vol. 12, no. 9, pp. 38–48, Sep. 2015.

[17] Z. Yuan, G. Yu, W. Li, Y. Yuan, X. Wang, and J. Xu, "Multi-user shared access for Internet of Things," in *Proc. IEEE 83rd Veh. Technol. Conf. (VTC Spring)*, May 2016, pp. 1–5.

[18] S. Chen, B. Ren, Q. Gao, S. Kang, S. Sun, and K. Niu, "Pattern division multiple access—A novel nonorthogonal multiple access for fifth-generation radio networks," *IEEE Trans. Veh. Technol.*, vol. 66, no. 4, pp. 3185–3196, Apr. 2017.

[19] J. Li, X. Wu, and R. Laroia, *OFDMA Mobile Broadband Communications: A Systems Approach*. Cambridge, U.K.: Cambridge Univ. Press, 2013.

[20] B. Farhang-Boroujeny, "OFDM versus filter bank multicarrier," *IEEE Signal Process. Mag.*, vol. 28, no. 3, pp. 92–112, May 2011.

[21] N. Michailow *et al.*, "Generalized frequency division multiplexing for 5th generation cellular networks," *IEEE Trans. Commun.*, vol. 62, no. 9, pp. 3045–3061, Sep. 2014.

[22] V. Vakilian, T. Wild, F. Schaich, S. ten Brink, and J. F. Frigon, "Universal-filtered multi-carrier technique for wireless systems beyond LTE," in *Proc. IEEE Globecom Workshops (GC Wkshps)*, Dec. 2013, pp. 223–228.

[23] L. Zhang, A. Ijaz, P. Xiao, M. M. Molu, and R. Tafazolli, "Filtered OFDM systems, algorithms, and performance analysis for 5G and beyond," *IEEE Trans. Commun.*, vol. 66, no. 3, pp. 1205–1218, Mar. 2017.

[24] X. Gao *et al.*, "An efficient digital implementation of multicarrier CDMA system based on generalized DFT filter Banks," *IEEE J. Sel. Areas Commun.*, vol. 24, no. 6, pp. 1189–1198, Jun. 2006.

[25] X. Zhang, M. Li, H. Hu, H. Wang, B. Zhou, and X. You, "DFT spread generalized multi-carrier scheme for broadband mobile communications," in *Proc. IEEE 17th Int. Symp. Pers. Indoor Mobile Radio Commun.*, Sep. 2006, pp. 1–5.

[26] T. Yunzheng, L. Long, L. Shang, and Z. Zhi, "A survey: Several technologies of non-orthogonal transmission for 5G," *China Commun.*, vol. 12, no. 10, pp. 1–15, Oct. 2015.

[27] Y. Cai, Z. Qin, F. Cui, G. Y. Li, and J. A. McCann, "Modulation and multiple access for 5G networks," *IEEE Commun. Surveys Tuts.*, vol. 20, no. 1, pp. 629–646, 1st Quart., 2017.

[28] B. Wang, K. Wang, Z. Lu, T. Xie, and J. Quan, "Comparison study of non-orthogonal multiple access schemes for 5G," in *Proc. IEEE Int. Symp. Broadband Multimedia Syst. Broadcast.*, Jun. 2015, pp. 1–5.
[29] W. Yuan, C. Zhang, and K. Qiu, "Transmission performance of NOMA and FBMC-based IM/DD RoF-5G communications," in *Proc. Int. Topical Meeting Microw. Photon. (MWP)*, Oct. 2017, pp. 1–4.
[30] A. Mokdad, P. Azmi, and N. Mokari, "Radio resource allocation for heterogeneous traffic in GFDM-NOMA heterogeneous cellular networks," *IET Commun.*, vol. 10, no. 12, pp. 1444–1455, Aug. 2016.
[31] L. Wen *et al.*, "Joint sparse graph for FBMC/OQAM systems," *IEEE Trans. Veh. Technol.*, to be published. [Online]. Available: https://ieeexplore.ieee.org/document/8304665/
[32] M. Li, Y. Rui, and Z. Bu, *Fourier Transform Based Transmission Systems for Broadband Wireless Communications*. Rijeka, Croatia: InTech, 2011, ch. 11, pp. 203–226. [Online]. Available: https://www.intechopen.com/
[33] B. Ren, Y. Wang, X. Dai, K. Niu, and W. Tang, "Pattern matrix design of PDMA for 5G UL applications," *China Commun.*, vol. 13, no. 2, pp. 159–173, Jan. 2017.
[34] R. Hoshyar, F. P. Wathan, and R. Tafazolli, "Novel low-density signature for synchronous CDMA systems over AWGN channel," *IEEE Trans. Signal Process.*, vol. 56, no. 4, pp. 1616–1626, Apr. 2008.
[35] Y. Rui, H. Hu, H. Yi, H.-H. Chen, and Y.-M. Huang, "Frequency domain discrete Fourier transform spread generalized multi-carrier system and its performance analysis," *Comput. Commun.*, vol. 32, no. 3, pp. 456–464, 2009.
[36] M. Li and X. Zhang, "Performance analysis of DFT spread generalized multi-carrier systems," *Sci. China F, Inf. Sci.*, vol. 52, no. 12, p. 2385, Dec. 2009.
[37] Y. Rui, M. Li, Q. Zhou, X. Zhang, H. Yi, and H. Hu, "SINR performance analysis of DFT spread generalized multi-carrier system," *J. Commun.*, vol. 29, no. 6, pp. 51–56, 2008.
[38] *Study on New Radio Access Technology Physical Layer Aspects*, document TR 38.802, 3GPP, Mar. 2017.
[39] *Technical Specification Group Radio Access Network*, document TR 25.890, 3GPP, 2002.
[40] C. P. Robert and G. Casella, *Monte Carlo Statstical Methods*. Springer, 2004.
[41] H. Silverman, "An introduction to programming the Winograd Fourier transform algorithm (WFTA)," *IEEE Trans. Acoust., Speech, Signal Process.*, vol. ASSP-25, no. 2, pp. 152–165, Apr. 1977.
[42] X. Zhang, *Matrix Analysis and Applications*, 2nd ed. Beijing, China: Tsinghua Univ. Press, 2013.

**XIN BIAN** received the B.S. degree in telecommunications engineering from Anhui Normal University in 2011. He is currently pursuing the Ph.D. degree in communication and information systems with the Nanjing University of Posts and Telecommunications. His research interests are in the areas of filter bank modulation and multiple access techniques.

**JIE TANG** received the B.S. degree in electronic science and technology from Beijing Jiaotong University in 2009. He is currently pursuing the Ph.D. degree in communication and information systems with the Shanghai Advanced Research Institute, Chinese Academy of Sciences. His research interests include synchronization, MIMO precoding, and MIMO detection.

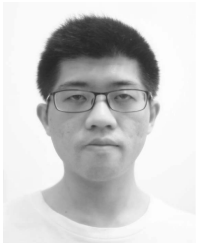

**HONG WANG** received the B.S. degree in telecommunications engineering from Jiangsu University, Zhenjiang, China, in 2011, and the Ph.D. degree from the Department of Telecommunications Engineering, Nanjing University of Posts and Telecommunications (NUPT), Nanjing, China, in 2016.

From 2014 to 2015, he was a Research Assistant with the Department of Electronic Engineering, City University of Hong Kong, Hong Kong. From 2016 to 2018, he was a Senior Research Associate with the State Key Laboratory of Millimeter Waves, Department of Electronic Engineering, City University of Hong Kong. Since 2016, he has also been an Instructor with the Department of Telecommunication Engineering, NUPT. His research interests are in the area of broadband wireless communication, particularly in interference analysis and management in HetNets.

**MINGQI LI** received the Ph.D. degree in communication and information systems from Shanghai Jiao Tong University in 2004. He is currently a Professor and the Deputy Director of the Research Center of Wireless Technologies for New Media, Shanghai Advanced Research Institute, Chinese Academy of Sciences. His research interests include filter bank modulation techniques, next-generation broadcasting-wireless, and 5G wireless communications.

**RONGFANG SONG** received the B.S. and M.S. degrees from the Nanjing University of Posts and Telecommunications (NUPT), Nanjing, China, in 1984 and 1989, respectively, and the Ph.D. degree from Southeast University, Nanjing, in 2001, all in electronic engineering.

From 2002 to 2003, he was a Research Associate with the Department of Electronic Engineering, City University of Hong Kong, Hong Kong. Since 2002, he has been a Professor with the Department of Telecommunications Engineering, NUPT. His research interests are in the area of broadband wireless communication, with current focus on interference management in HetNets, non-orthogonal multiple access, and compressed sensing-based signal processing.